Cooperative Self-Assembly of Pyridine-2,6-Diimine-Linked Macrocycles into Mechanically Robust Nanotubes

Michael J. Strauss[1], Darya Asheghali[2], Austin M. Evans[1], Rebecca L. Li[1], Anton D. Chavez[1,3], Chao Sun[1,3], Matthew L. Becker[2,*], and William R. Dichtel[1,*]

[1]Department of Chemistry, Northwestern University, 2145 Sheridan Road, Evanston, Illinois 60208, United States

[2]Department of Polymer Science, The University of Akron, Akron, Ohio 44325, United States

[3]Department of Chemistry and Chemical Biology, Baker Laboratory, Cornell University, Ithaca, New York 14853, United States

Supporting Information Placeholder

ABSTRACT: Nanotubes assembled from macrocyclic precursors offer a unique combination of low dimensionality, structural rigidity, and distinct interior and exterior microenvironments. Usually the weak stacking energies of macrocycles limit the length or strength of the resultant nanotubes. Imine-linked macrocycles were recently found to assemble into high-aspect ratio (>10^3), lyotropic nanotubes in the presence of excess acid. Yet these harsh conditions are incompatible with many functional groups and processing methods, and lower acid loadings instead catalyze macrocycle degradation. Here we report pyridine-2,6-diimine-linked macrocycles that assemble into high-aspect ratio nanotubes in the presence of less than 1 equiv of CF_3CO_2H per macrocycle. Analysis by gel permeation chromatography and fluorescence spectroscopy revealed a cooperative self-assembly mechanism. Nanofibers obtained by touch-spinning the pyridinium-based nanotubes exhibit Young's moduli of 1.48 GPa, which exceeds that of many synthetic polymers and biological filaments. These findings will enable the design of structurally diverse nanotubes from synthetically accessible macrocycles.

Introduction

Nanotubes assembled from macrocyclic precursors offer unique properties that stem from their low dimensionality, structural rigidity, and tunable microenvironments through rational synthetic design.[1-5] The corresponding macrocyclic building blocks are accessed using molecular design principles, allowing for control over the diameter, interior microenvironment, and chemical functionality of the corresponding nanotube. Despite these tailorable properties, cohesive forces between macrocycles are usually too weak to produce nanotubes with the high aspect ratios (>10^3) of carbon nanotubes and biological filaments.[6] Generally, stacked macrocycles exhibit low aspect ratios (~10), or are stabilized by bundling.[7] However, macrocycles decorated with alkyl or alkyloxy side chains form bulk liquid crystalline phases that can be oriented through host-guest interactions with metal ions or molecular compounds.[4] Previously, Shionoya and coworkers and Tanaka and coworkers synthesized macrocycles containing 1,10-phenanthroline and bis(salicylidene)-*o*-phenylenediamine moieties, respectively, which assembled into nanotubes upon binding transition metals.[8-9] We recently reported hexagonal macrocyclic analogues of two-dimensional imine-linked covalent organic frameworks, which assemble into high-aspect ratio, lyotropic nanotubes upon protonation of the imine linkages.[10-11] One of the unique aspects of this system is that a large excess of CF_3CO_2H induced assembly, yet lower acid loadings catalyzed macrocycle hydrolysis. However, these characteristics are detrimental to accessing functionalized structures, as well as processing and aligning the nanotubes. Designing macrocycles that assemble into nanotubes in the presence of stoichiometric quantities of acid is needed to fully leverage their potential.

Here we report the rational design of macrocycles that assemble into high-aspect ratio nanotubes with as little as 0.4 equiv of CF_3CO_2H. By including a pyridine moiety within the macrocyclic framework, which is more basic than the imine linkages, self-assembly is driven by the formation of pyridinium ions, rather than hydrolytically unstable iminium ions.[11] Touch-spinning of nanotube solutions provided nanofibers with Young's moduli of 1.48 GPa, which exceeds those of several synthetic polymers and actin filaments.[12-14] These robust mechanical properties indicate the strong stacking interactions of these systems, which are the first non-covalent assemblies amenable to the processing technique.[15] Using synthetic chemistry to target persistent, yet reversible molecular assemblies is an emerging challenge in materials science.[16-17] Developing general approaches towards this goal is imperative to form nanostructures with designed and dynamic emergent functions. [18-20]

Results and Discussion

A bifunctional aryl amine, containing a solubilizing decyloxy side chain, was condensed with both 2,6-pyridinedicarboxaldehyde (**MC 1**) and isophthalaldehyde (**MC 2**) to yield [3+3] macrocycles in high yields (91% and 80%, respectively) with smaller pore sizes than previous reports (Figure 1, Scheme S7 and S8). [10-11] Both macrocycles exhibit single narrow peaks in the gel permeation chromatography (GPC) traces, as well as peaks in the matrix assisted laser desorption ionization mass-spectrometry (MALDI-MS) spectra corresponding to the desired [3+3] product (See Supporting Information).

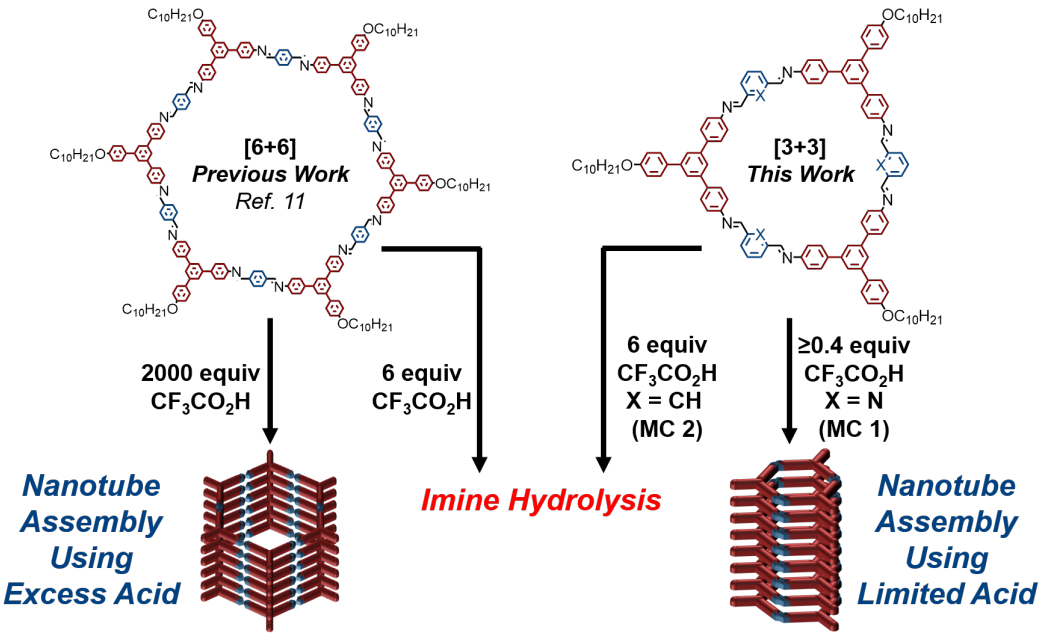

Figure 1. Impact of linkage chemistry on macrocycle topology and assembly behavior. (Left) [6+6] macrocycles constructed from bifunctional aryl amine and terepthalaldehyde, which assemble into high-aspect ratio nanotubes in the presence of a large excess of acid, but to unstable to lower amounts of added acid.[11] (Right) [3+3] macrocycles, constructed from aromatic 1,3-dialdehydes, which assemble into nanotubes in the presence of as little as 0.4 equiv of CF_3CO_2H when pyridine moieties are incorporated into the macrocycle. Otherwise identical [3+3] macrocycles lacking pyridines have similar assembly and degradation behavior as the previously reported [6+6] macrocycles.

MC 1 assembles into high-aspect ratio nanotubes in the presence of 3 equiv of CF_3CO_2H (Figure 2A) because it contains pyridines, which are significantly more basic than imines. In contrast, **MC 2** requires a large excess of acid to assemble, similar to previous imine-linked macrocycles (Figure 2A).[11] Acidifying and drop-casting solutions of **MC 1** in THF with 0.3 mM tetrabutylammonium perchlorate (TBAP), with either 3 or 2000 equiv of CF_3CO_2H depicted the formation of bundles of approximately 15-25 nanotubes across via atomic force microscopy (AFM, Figures 2B and S23-S24). Furthermore, the degree of bundling was confirmed through scanning electron microscopy (SEM, Figures S30 and S31). In contrast, **MC 2** required a large excess of CF_3CO_2H (2000 equiv) to assemble, and a similar degree of bundling was observed (Figure 2E and S29). To confirm the presence of organized macrocycles within the self-assemblies, grazing-incidence wide-angle x-ray scattering (GI-WAXS) measurements were taken on a drop-cast film of nanotubes. Based on the anisotropy of the scattering in the two-dimensional diffraction pattern, it was determined that the nanotubes lie parallel to the surface, as seen in the AFM and SEM images (Figures S36-37 and S41). Additionally, the extracted 1D pattern is in good agreement with a refined diffraction pattern corresponding to macrocycle assembly (Figures 2D and S34-35). Although assembly of **MC 1** was observed upon addition of 3 equiv of CF_3CO_2H, enough to protonate all of the pyridines, it is possible that all pyridine moieties need not be protonated to yield an assembled supramolecular structure. Attempts to assemble a solution of **MC 1** in THF with 0.3 mM TBAP with 0 equiv of CF_3CO_2H failed to produce an extended structure, as evident by the inability to observe nanotubes via AFM or GI-WAXS, demonstrating the necessity for protonation (Figures S28 and S40). However, samples of **MC 1** acidified with 1 or 2 equiv of CF_3CO_2H assembled similarly to the samples acidified with higher acid concentrations (Figure 2A, See Supporting Information).

The assembly of **MC 1** at low acid (≤3 equiv CF_3CO_2H) loadings confers the same acid stability to these macrocycles that was observed for **MC 2** and other systems in the presence of excess acid.[11] To demonstrate the protection of the imine linkages of **MC 1** upon the addition of 1-2000 equiv of CF_3CO_2H, MALDI-MS spectra were taken following acid neutralization, which showed recovery of the initial macrocycle, with no discernible peaks corresponding to macrocycle degradation products (Figures 2C and S47-50). While recovery of the initial macrocycle was demonstrated following the neutralization of nanotubes assembled from **MC 2** with 2000 equiv of CF_3CO_2H, analysis of a neutralized solution of **MC 2** (Figure 2C) that had been acidified with 6 equiv of CF_3CO_2H showed the presence of macrocycle fragments, with no peaks corresponding to the initial macrocycle (Figures S45-46). The hydrolysis of **MC 2** under low acid loadings, along with the lack of extended structures found by AFM or GI-WAXS, demonstrates the inability of **MC 2** to assemble under low acid loadings (Figures S22 and S42). Overall, macrocycle assembly into nanotubes is shown to protect the imine linkages from hydrolysis, consistent with previous reports.[11] In addition to assembly preventing hydrolysis of imine-linked macrocycles under low acid loadings, the inclusion of the more basic pyridine moiety causes assembly to occur upon pyridinium ion formation, rather than hydrolytically unstable iminium ions (Figure 2A).

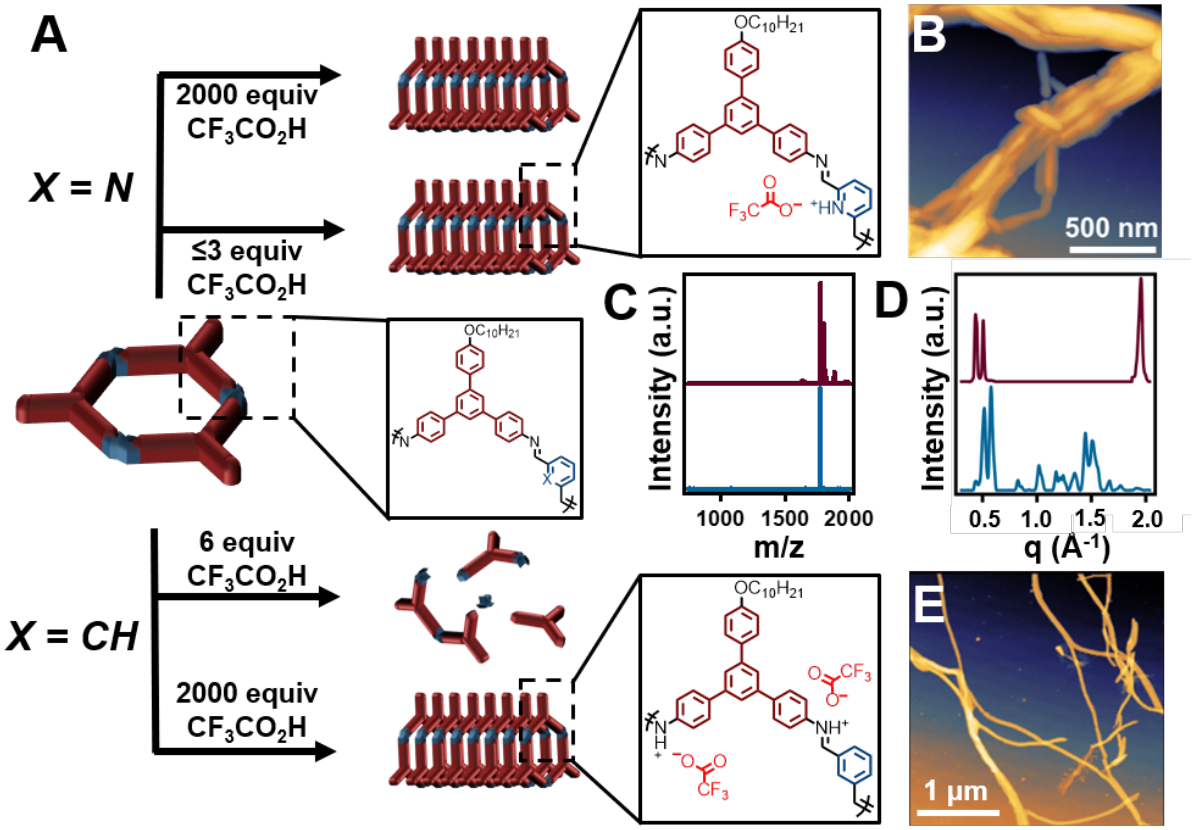

Figure 2. Linker effects on the assembly of imine-linked macrocycles. (A) Scheme depicting the linker effects on the assembly capability of imine-linked macrocycles. (B) Atomic force micrograph of nanotubes assembled from **MC 1** macrocyles acidified with 3 equiv of CF_3CO_2H. (C) MALDI-MS spectra resulting from the neutralization of nanotubes assembled from **MC 1** with 2 equiv of CF_3CO_2H (maroon), and from **MC 2** assembled with 2000 equiv of CF_3CO_2H (blue). No imine hydrolysis products are observed in either spectra. (D) 1D-WAXS patterns of nanotubes assembled from **MC 1** macrocycles (maroon) and **MC 2** (blue). (E) Atomic force micrograph of nanotubes assembled from **MC 2** macrocycles acidified with 2000 equiv of CF_3CO_2H.

MC 1 undergoes cooperative assembly at sub-stoichiometric acid loadings as determined by GPC and fluorescence spectroscopy. Although nanotubes were observed in the presence of only 1 equiv of CF_3CO_2H, it was pertinent to understand whether the acid was triply protonating a small subset of macrocycles, leading to a low yield of nanotubes. Alternatively, one or fewer protonation events per macrocycle might drive nanotube formation in high yield. Tracing macrocycle consumption as a function of acid loading made use of the in-line refractive index (RI) detector of the GPC, which was calibrated to determine the amount of macrocycle in solution (Figure S59). Solutions of **MC 1** (0.5 mg/mL in THF with 0.3 mM TBAP), were acidified with varying amounts of CF_3CO_2H, allowed to equilibrate for 2 hours, passed through a 0.4 μm syringe filter to remove any assembled nanotubes, and analyzed via GPC. The decrease in RI intensity was attributed to macrocycles that were incorporated into nanotubes (Figure S60-S61). Based on this analysis it was determined that 75% of the macrocycles in solution were incorporated into the nanotubes upon addition of 0.4 equiv of CF_3CO_2H (Figures 3A and S60-S61). Neutralization of the acid and analysis via MALDI-MS showed recovery of **MC 1**, demonstrating that the decrease in RI was not a function of macrocycle hydrolysis (Figure S51). We also noted that nanotube formation was associated with decreased emission of the **MC 1** fluorophore. This phenomenon enabled an independent measure of the yield of macrocycle assembly as a function of added acid. Solutions of **MC 1** have an emission feature centered at 430 nm (λ_{ex} = 330 nm) whose intensity decreased upon addition of ≤1 equiv of CF_3CO_2H (Figure 3A). The amount of fluorescence quenching (I/I_0) as a function of acid loading correlated extremely well to the residual concentration of free macrocycles determined in the GPC measurements. AFM images of the solutions used in the GPC and fluorescence experiments that contained 0.4 equiv CF_3CO_2H confirmed the presence of high-aspect ratio nanotubes (Figure S27), further indicating that these experiments were performed under conditions in which macrocycles assemble.

A Stern-Volmer analysis of the quenching of **MC 1** and a tris(imine) model compound that is incapable of assembly, yet stable to sub-stoichiometric quantities of CF_3CO_2H, further demonstrates that nanotube formation by **MC 1** is highly cooperative. Titration of the model compound, which was derived from 1,3,5-tris(4-aminophenyl)benzene and 2-pyridinecarboxaldehyde, with CF_3CO_2H and monitoring fluorescence at 430 nm after excitation at 330 nm yielded no observable quenching (Scheme S6, Figure S70). In contrast, Stern-Volmer analysis of the fluorescence data demonstrated that **MC 1** had a relatively high quenching constant (K_{SV} = 5.97), whereas that of the model compound is close to zero (K_{SV} = 0.08, Figure 3B). Additionally, the UV-Vis and fluorescence spectra of **MC 1** and the tris(imine) model compound demonstrate that the dominant fluorophore is the triphenylbenzene core of the bifunctional aryl amine monomer (Figure S71). The Stern-Volmer quenching constant of **MC 1** of 5.97, suggests that each pyridinium quenches 6 fluorophores, or 2 complete macrocycles. This finding is consistent with a cooperative assembly process (Figure

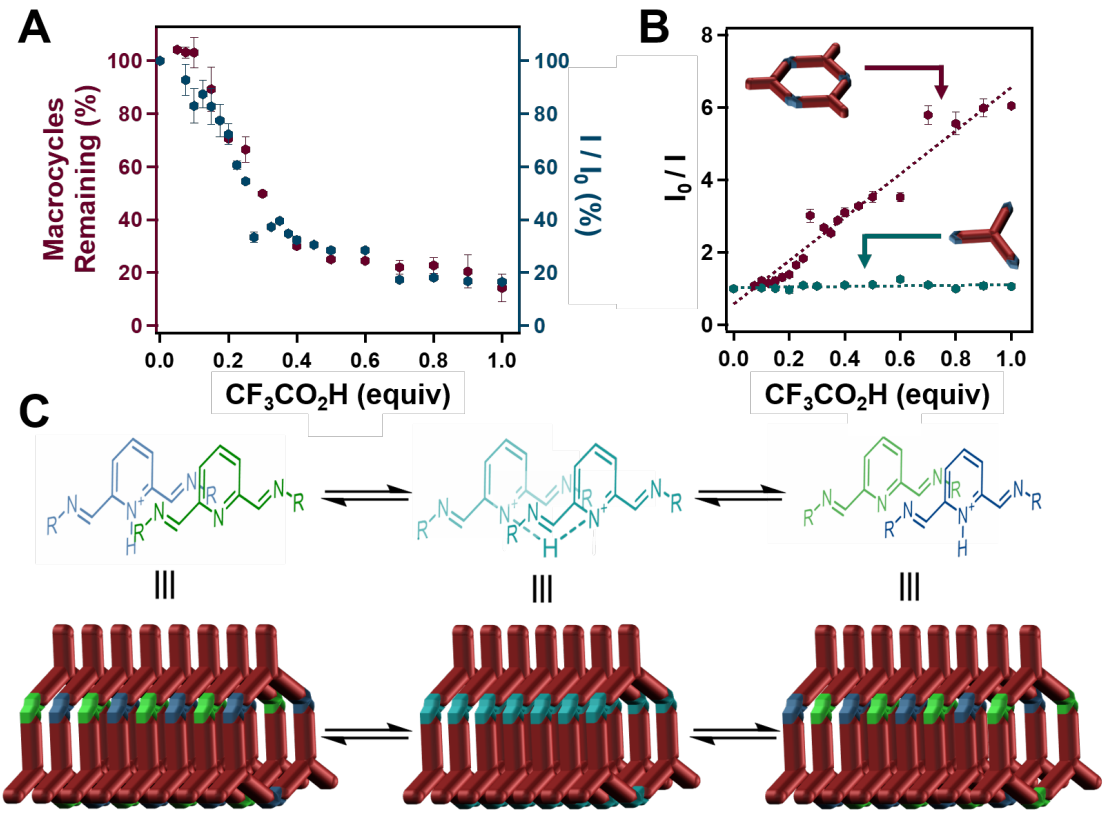

Figure 3. Probing the cooperativity of assembly as a function of acid loading. (A) Overlay of macrocycle consumption (as determined by GPC) and fluorescence intensity (λ_{ex} = 330 nm, λ_{em} = 430 nm) of acidified solutions of **MC 1**. (B) Stern-Volmer plot of fluorescence quenching of **MC 1** and a synthetic model as a response to sub-stoichiometric acid loadings. (C) Schematic of proposed assembly mechanism in which macrocycles which have been protonated once, and macrocyles that have not been protonated at all, alternate within the supramolecular assembly.

3C). Additionally, when these findings are evaluating alongside the above GPC, AFM, and MALDI-MS data, it is clear that the observed quenching is a direct result of nanotube formation rather than the formation of a disallowed emissive state, or intramolecular charge transfer.

Nanotubes assembled from **MC 1**, along 0.5 wt% poly(ethylene oxide) (PEO) were touch-spun into nanofibers (NT-NF) supported by non-covalent interactions. In the touch-spinning of fibers from polymer samples, a solution of polymer is pushed through a tube by a syringe pump, and the polymer droplet ejects from the tip of a nozzle in close proximity to bars on a rotating disk. As the disk rotates, the tip of the bar touches the droplet at the tip of the nozzle, resulting in the formation of a liquid bridge. As the disk continues to rotate, the liquid bridge stretches and solvent evaporates, thereby allowing the fiber to solidify (Figure 4A).[15] Characterization of the NT-NF by AFM, transmission electron microscopy (TEM), and SEM highlight their high-aspect ratio and uniform diameter (Figures S74-S81). Infrared spectroscopy of the resulting fibers shows a peak at 1610 cm^{-1} corresponding to the imine linkages of the macrocycles (Figure S82-S83). Additionally, deprotonation of the pyridinium moiety of the nanotubes, followed by a brief bath sonication, yielded recovery of **MC 1** as determined by MALDI-MS, with no smaller macrocycle fragments; thus demonstrating that the mechanical force exhibited by touch-spinning does not alter the chemical composition of the nanotube solution (Figure S84). The process of touch-spinning necessitates molecular cohesion between monomeric building blocks. While traditional touch-spinning takes advantage of covalent bonds along a polymer backbone, the touch-spinning of NT-NF relies on cohesion as a function of noncovalent interactions between macrocycles. As such, the attempted touch-spinning of a neutral solution of **MC 1** with 0.5 wt% PEO fails to yield nanofibers (Figure S86).

Despite being supported by non-covalent interactions, NT-NF demonstrated a Young's modulus exceeding that of several covalently linked polymers and biological filaments. Traditionally, touch-spinning is used to increase the mechanical properties of the polymer samples in a variety of applications, from the design of new composite materials, to the development of biomimetic scaffolds suitable for artificial bones and organs.[15] NT-NF demonstrated a higher Young's modulus (1.48 ± 0.31 GPa) than touch-spun fibers of PEO (0.18 ± 0.05 GPa), polycaprolactone (PCL) (0.02 ± 0.00 GPa), and a poly(ester urea) (PEU)[21] (0.68 ± 0.04 GPa) (Figure 4C, Tables S11-S13). In addition to its higher Young's modulus than touch-spun nanofibers of covalent polymers, the nanotube nanofibers demonstrate a Young's modulus higher than biological materials of interest, such as: actin (1.30 GPa),[13-14] collagen type I (0.10-0.36 GPa),[22] and tubulin dimers (0.6 GPa).[23] The high modulus of the NT-NF is presumably due to the interplay of multiple intramolecular forces, such as the electrostatic interactions that govern the initial assembly event, the hydrophobic interactions of the decyloxy side chains that are forced into close proximity, as well as the π-π interactions present from macrocycle self-assembly.[24-28]

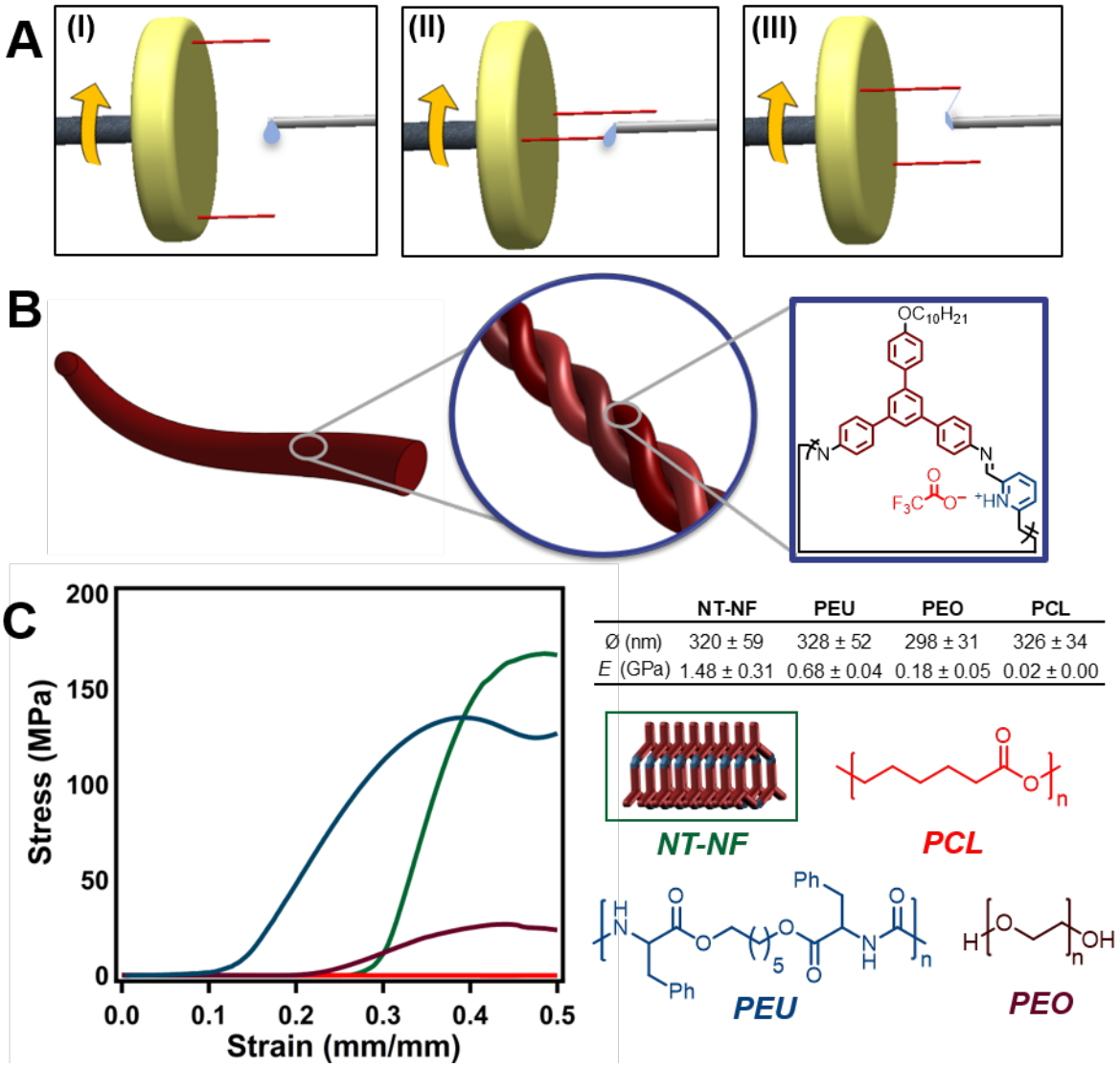

	NT-NF	PEU	PEO	PCL
Ø (nm)	320 ± 59	328 ± 52	298 ± 31	326 ± 34
E (GPa)	1.48 ± 0.31	0.68 ± 0.04	0.18 ± 0.05	0.02 ± 0.00

Figure 4. Touch-spinning of nanotube nanofibers. (A) Schematic of the touch-spinning process in which (I) a droplet of a polymer solution ejects from the tip of the nozzle, (II) the bar attached to the spinneret touches the polymer droplet at the tip of the nozzle, and (III) as the spinneret rotates, the droplet stretches to form a liquid bridge which solidifies into a fiber. (B) Schematic of the structure of the nanofiber that results from the touch-spinning of a nanotube solution. (C) Results from the mechanical testing of touch-spun nanofibers derived from NT-NF, along with several covalent polymer benchmarks.

Conclusions

This work establishes that imine-linked macrocycles, which are easily designed and prepared from simple and modular components, assemble into high-aspect ratio nanotubes under mild conditions when they contain easily protonatable groups. The enhanced basicity of the pyridine moiety compared to the imine linkages enables assembly to proceed through the formation of pyridinium ions, instead of the hydrolytically unstable iminium ions. The assembly of **MC 1** under sub-stoichiometric acid loadings is highly cooperative, as demonstrated by GPC measurements of macrocycle disappearance as well as fluorescence spectroscopy. The assembled nanotubes were processed into NT-NF via touch-spinning. The resulting fibers demonstrated a Young's modulus of 1.48 GPa, exceeding that of several covalently linked polymers and biological filaments. Together, these findings demonstrate a general design principle for the synthesis of macrocycle assembles under mild conditions, as well as the ability to touch-spin nanofibers of sufficiently robust supramolecular assemblies.

ASSOCIATED CONTENT

Supporting Information

The Supporting Information is available free of charge on the ChemRxiv Preprint Server:

Experimental procedures and additional characterization data (PDF)

Corresponding Author

WRD: wdichtel@northwestern.edu
MLB: becker@uakron.edu

Notes

The authors declare no competing financial interests

ACKNOWLEDGMENT

This work was funded by the Army Research Office through the Multidisciplinary University Research Initiative (MURI; W911NF-15-1-0447, to W.R.D.). M.J.S. was supported by the National Science Foundation (NSF) through the Graduate Research Fellowship Program (GRFP) under Grant No. (DGE-1842165.). A.M.E. was supported by the National Science Foundation (NSF) through the Graduate Research Fellowship Program (GRFP) under Grant No. (DGE-1324585). This work made use of the Integrated Molecular Structure Education and Research Center (IMSERC) at Northwestern University, which has received support from the National Science Foundation (NSF; CHE-1048773), the Soft and Hybrid Nanotechnology Experimental (SHyNE) Resource (NSF; NNCI-1542205), the State of Illinois, and the International Institute for Nanotechnology (IIN). This work also made use of the Scanned Probe Imaging and Development (SPID), and the Electron Probe Instrumentation Center (EPIC), facilities of Northwestern University's Atomic and Nanoscale Characterization Experiment Center (NUANCE), which has received support from the Soft and Hybrid Nanotechnology Experimental (SHyNE) Resource (NSF; ECCS-1542205); the MRSEC program (NSF; DMR-1720139) at the Materials Research Center; the International Institute for Nanotechnology (IIN); the Keck Foundation; and the State of Illinois. This work was also supported by the Northwestern University Keck Biophysics Facility and a Cancer Center Support Grant (NCI CA060553). Parts of this work were performed at the DuPoint-Northwestern-Dow Collaborative Access Team (DND-CAT) located at Sector 5 of the Advanced Photon Source (APS) at Argonne National Lab. This research used resources of the Advanced Photon Source and the Center for Nanoscale Materials, both U.S. Department of Energy (DOE) Office of Science User Facilities operated for the DOE Office of Science by Argonne National Laboratory under Grant No. (DGE-1324585). M.L.B. acknowledges support from the Ohio Third Frontier (Akron Functional Materials Center). We acknowledge Prof. Todd Blackledge and Angela Alicea for their assistance with the UTM NanoBionix tensile tester. We acknowledge Thomas Fitzsimons (Whiff L.L.C.) for preparing the touch-spinning prototype. We acknowledge Joseph Accardo for helpful discussions and Prof. Julia Kalow for the use of her GPC instrument.

REFERENCES

1. Iijima, S., Helical microtubules of graphitic carbon. *Nature* **1991,** *354*, 56.

2. Fischer, M.; Lieser, G.; Rapp, A.; Schnell, I.; Mamdouh, W.; De Feyter, S.; De Schryver, F. C.; Höger, S., Shape-Persistent Macrocycles with Intraannular Polar Groups: Synthesis, Liquid Crystallinity, and 2D Organization. *J. Am. Chem. Soc.* **2004,** *126* (1), 214-222.

3. Sato, K.; Itoh, Y.; Aida, T., Columnarly Assembled Liquid-Crystalline Peptidic Macrocycles Unidirectionally Orientable over a Large Area by an Electric Field. *J. Am. Chem. Soc.* **2011,** *133* (35), 13767-13769.

4. Stępień, M.; Donnio, B.; Sessler, J. L., Supramolecular Liquid Crystals Based on Cyclo[8]pyrrole. *Angew. Chem. Int. Ed.* **2007,** *46* (9), 1431-1435.

5. Zhang, J.; Moore, J. S., Nanoarchitectures. 6. Liquid Crystals Based on Shape-Persistent Macrocyclic Mesogens. *J. Am. Chem. Soc.* **1994,** *116* (6), 2655-2656.

6. Fukino, T.; Joo, H.; Hisada, Y.; Obana, M.; Yamagishi, H.; Hikima, T.; Takata, M.; Fujita, N.; Aida, T., Manipulation of Discrete Nanostructures by Selective Modulation of Noncovalent Forces. *Science* **2014,** *344* (6183), 499-504.

7. Bong, D. T.; Clark, T. D.; Granja, J. R.; Ghadiri, M. R., Self-Assembling Organic Nanotubes. *Angew. Chem. Int. Ed.* **2001,** *40* (6), 988-1011.

8. Kuritani, M.; Tashiro, S.; Shionoya, M., Organic and Organometallic Nanofibers Formed by Supramolecular Assembly of Diamond-Shaped Macrocyclic Ligands and PdII Complexes. *Chem. Asian J.* **2013,** *8* (7), 1368-1371.

9. Kawano, S.-i.; Ishida, Y.; Tanaka, K., Columnar Liquid-Crystalline Metallomacrocycles. *J. Am. Chem. Soc.* **2015,** *137* (6), 2295-2302.

10. Chavez, A. D.; Evans, A. M.; Flanders, N. C.; Bisbey, R. P.; Vitaku, E.; Chen, L. X.; Dichtel, W. R., Equilibration of Imine-Linked Polymers to Hexagonal Macrocycles Driven by Self-Assembly. *Chem. Eur. J.* **2018,** *24* (16), 3989-3993.

11. Sun, C.; Shen, M.; Chavez, A. D.; Evans, A. M.; Liu, X.; Harutyunyan, B.; Flanders, N. C.; Hersam, M. C.; Bedzyk, M. J.; Olvera de la Cruz, M.; Dichtel, W. R., High aspect ratio nanotubes assembled from macrocyclic iminium salts. *Proc. Natl. Acad. Sci. U.S.A.* **2018**.

12. Engineering Toolbox. *Young's Modulus- Tensile and Yield Strength for Common Materials*. https://www.engineeringtoolbox.com/young-modulus-d_417.html. (accessed March 2019).

13. Higuchi, H.; Yanagida, T.; Goldman, Y. E., Compliance of thin filaments in skinned fibers of rabbit skeletal muscle. *Biophys. J.* **1995,** *69* (3), 1000-1010.

14. Janmey, P.; Tang, J.; F. Schmidt, C., *Actin Filaments*. 1999.

15. Tokarev, A.; Asheghali, D.; Griffiths, I. M.; Trotsenko, O.; Gruzd, A.; Lin, X.; Stone, H. A.; Minko, S., Touch- and Brush-Spinning of Nanofibers. *Adv. Mater.* **2015,** *27* (41), 6526-6532.

16. Song, W.; Kinloch, I. A.; Windle, A. H., Nematic Liquid Crystallinity of Multiwall Carbon Nanotubes. *Science* **2003,** *302* (5649), 1363-1363.

17. Aida, T.; Meijer, E. W.; Stupp, S. I., Functional Supramolecular Polymers. *Science* **2012,** *335* (6070), 813-817.

18. Chen, X.; Gerasopoulos, K.; Guo, J.; Brown, A.; Wang, C.; Ghodssi, R.; Culver, J. N., Virus-Enabled Silicon Anode for Lithium-Ion Batteries. *ACS Nano* **2010,** *4* (9), 5366-5372.

19. Keber, F. C.; Loiseau, E.; Sanchez, T.; DeCamp, S. J.; Giomi, L.; Bowick, M. J.; Marchetti, M. C.; Dogic, Z.; Bausch, A. R., Topology and dynamics of active nematic vesicles. *Science* **2014,** *345* (6201), 1135-1139.

20. Niu, Z.; Liu, J.; Lee, L. A.; Bruckman, M. A.; Zhao, D.; Koley, G.; Wang, Q., Biological Templated Synthesis of Water-Soluble Conductive Polymeric Nanowires. *Nano Lett.* **2007,** *7* (12), 3729-3733.

21. Yu, J.; Lin, F.; Lin, P.; Gao, Y.; Becker, M. L., Phenylalanine-Based Poly(ester urea): Synthesis, Characterization, and in vitro Degradation. *Macromolecules* **2014,** *47* (1), 121-129.

22. Dutov, P.; Antipova, O.; Varma, S.; Orgel, J. P. R. O.; Schieber, J. D., Measurement of Elastic Modulus of Collagen Type I Single Fiber. *PLOS ONE* **2016,** *11* (1), e0145711.

23. Enemark, S.; Deriu, M. A.; Soncini, M.; Redaelli, A., Mechanical Model of the Tubulin Dimer Based on Molecular Dynamics Simulations. *J. Biomed. Eng.* **2008,** *130* (4), 041008-041008-7.

24. Adler-Abramovich, L.; Kol, N.; Yanai, I.; Barlam, D.; Shneck, R. Z.; Gazit, E.; Rousso, I., Self-Assembled Organic Nanostructures with Metallic-Like Stiffness. *Angew. Chem. Int. Ed.* **2010,** *49* (51), 9939-9942.

25. Azuri, I.; Meirzadeh, E.; Ehre, D.; Cohen, S. R.; Rappe, A. M.; Lahav, M.; Lubomirsky, I.; Kronik, L., Unusually Large Young's Moduli of Amino Acid Molecular Crystals. *Angew. Chem. Int. Ed.* **2015,** *54* (46), 13566-13570.

26. Galeotti, F.; Pisco, M.; Cusano, A., Self-assembly on optical fibers: a powerful nanofabrication tool for next generation "lab-on-fiber" optrodes. *Nanoscale* **2018,** *10* (48), 22673-22700.

27. Hartgerink, J. D.; Granja, J. R.; Milligan, R. A.; Ghadiri, M. R., Self-Assembling Peptide Nanotubes. *J. Am. Chem. Soc.* **1996,** *118* (1), 43-50.

28. Wang, S.; Chavez, A.; Thomas, S.; Li, H.; Flanders, N. C.; Sun, C.; Strauss, M. J.; Chen, L. X.; Markvoort, A. J.; Bredas, J.-L.; Dichtel, W. R., Pathway Complexity in the Stacking of Imine-linked Macrocycles Related to Two-Dimensional Covalent Organic Frameworks. *ChemRxiv* **2019**.

TOC Graphic

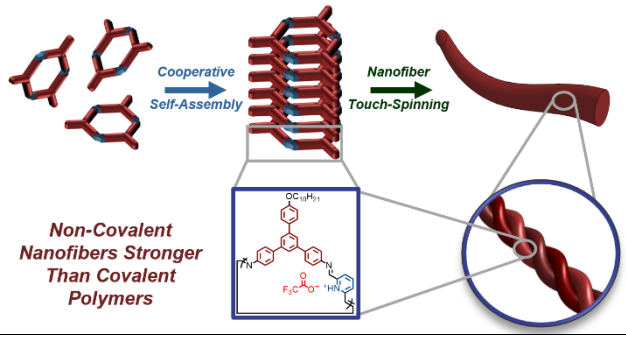
Cooperative
Self-Assembly
Nanofiber
Touch-Spinning
Non-Covalent
Nanofibers Stronger
Than Covalent
Polymers